Regularities of self-propagating high-temperature synthesis in the solid 8-hydroxyquinoline—chloramine B system

E. G. Klimchuk,[a] G. M. Avetisyan,[b] A. A. Khodak,[c] V. T. Minasyan,[d] K. G. Gazaryan,[d] A. S. Mukas'yan,[a] and A. G. Merzhanov[a]*

[a] *Institute of Structural Macrokinetics, Russian Academy of Sciences, 142432 Chernogolovka, Moscow Region, Russian Federation. Fax: +7 (095) 962 8040*

[b] *Institute of Fine Organic Chemistry, Armenian Academy of Sciences, 1 ul. P. Sevaka, 375044 Erevan, Armenia*

[c] *A. N. Nesmeyanov Institute of Organoelement Compounds, Russian Academy of Sciences, 28 ul. Vavilova, 117813 Moscow, Russian Federation. Fax: +7 (095) 135 5085*

[d] *Institute of Chemical Physics, Armenian Academy of Sciences, 5/2 ul. P. Sevaka, 375044 Erevan, Armenia*

The regularities of chemical reactions in solid 8-hydroxyquinoline—chloramine B mixtures were studied under conditions of organic self-propagating high-temperature synthesis (SHS), isothermal reaction, and thermal explosion in the 20—220 °C temperature range. Comprehensive physicochemical analysis and microstructural study of the reaction products were carried out. The temperature of SHS initiation (58 °C), the heat of the reaction (129±9 kJ mol^{-1}), the stoichiometric coefficient (1), the maximum temperature (T_{max} = 98—140 °C), and the velocity of SHS wave propagation (u = 0.15—0.55 mm s^{-1}) were determined. Depending on the ratio of the reactants (n), a low-temperature non-degenerate stable gasless mode ($n \leq 1$, T_{max} = 115 °C, E_a = 42 kcal mol^{-1}) and a high-temperature mode ($n > 1$, T_{max} = 140 °C, E_a = 0.4 kcal mol^{-1}) are possible for SHS. The SHS affords monohydroxy and monochloro derivatives of 8-hydroxyquinoline, benzenesulfonamide, NaCl, NaOH, and H_2O. The mechanism of the solid-phase reaction at temperatures below 58 °C includes surface, solid-phase, and gas-phase diffusion; that for SHS is capillary spreading of the hydroxyquinoline melt.

Key words: organic self-propagating high-temperature synthesis, autowave exothermal process, macrokinetics, 8-hydroxyquinoline, chloramine B, organic solid-state chemistry.

Previously[1,2] we demonstrated for the first time the possibility of autowave modes for exothermal syntheses of condensed organic compounds in mixtures of organic powders upon local initiation. In inorganic systems, these processes, known as "self-propagating high-temperature synthesis" (SHS), are widely used for the preparation of metal carbides, oxides, nitrides, *etc.*[3—6]

Taking the interaction of piperazine crystals with malonic acid as an example,[1,7] it has been found that the main characteristic features of this process are consistent with the general theory of SHS, but the process occurs at a lower temperature and at a lower rate.[8—14]

This work presents a detailed study of the autowave mode in the synthesis of organic compounds by redox interaction of 8-hydroxyquinoline (HQ) and chloramine B (CA) powders; the former compound is a reducing agent and the latter one is an oxidant.[15—17]

Experimental

The procedures of mode organization SHS and recording thermograms were described in detail previously.[1,7,11] The reactions were conducted under nearly adiabatic conditions. The sample size was 22×60 mm, the particle size in the powders was 0.2—0.16 mm, the [CA] : [HQ] molar ratio (n) was 1, the compacting pressure was 0.3 kg cm^{-2}, and the air pressure was 1 atm. The thermocouples were inserted into the sample at a distance of 2 cm from the initiation point.

The photographs of the reacting powder mixture located in a transparent cell were taken in reflected light by a Zenit-E camera at intervals of ~60 s.

The heats were determined based on the areas of the DTA peaks with allowance for the mass loss. Heat capacities of substances were estimated using published data.[18]

Analytically pure 8-hydroxyquinoline and chloramine B $PhSO_2NNaCl \cdot 3H_2O$ and reagent grade benzenesulfonamide (BSA) and NaCl were used. The content of chlorine in CA was 13.5% (the calculated value is 13.26%). 8-Hydroxyquinoline *N*-oxide was prepared by a known procedure.[19] HQ and CA were dried in a desiccator over $CaCl_2$ at 35 °C. Adsorption of reagent grade solvents was carried out by keeping thin layers of dry powders in a desiccator filled with the saturated vapor of a solvent at ~20 °C for several hours.

In view of the nonequilibrium character of the process and the fact that the chemical and phase composition of the product mixture may change during isolation by conventional procedures involving the use of solvents, analyses were carried

Translated from *Izvestiya Akademii Nauk. Seriya Khimicheskaya*, No. 12, pp. 2271—2284, December, 1999.

1066-5285/99/4812-2245 $22.00

out, whenever possible, without separation of the solid-phase product into components.

TLC was performed using Silufol plates (and a 1 : 1 CCl_4—ether mixture as the eluent). R_f were measured in relation to 8-hydroxyquinoline.[20]

Saturated aqueous solutions of samples were titrated by 0.02 *N* H_2SO_4 (against phenolphthalein).

The elemental analyses of the samples was carried out at the Institute of Fine Organic Chemistry, Armenian Academy of Sciences, and at A. N. Nesmeyanov Institute of Organoelement Compounds, RAS.

The X-ray diffraction patterns were recorded on a DRON-0.5 instrument. When studying the transformations of crystalline phases, the mixture of the powders was pressed to form ~3-mm thick round discs, from which parallelepipeds with dimensions 5×3×20 mm were cut out. IR spectra were measured on an IKS-29 instrument in pellets with KCl. ^{1}H NMR spectra were recorded on a Varian C-60 instrument (MeOH as the solvent and HMDS as the standard).

The ESR spectra of samples (0.2 g, 4 mm in diameter) were run on the thermal unit of a Varian E-104A spectrometer, which allowed maintenance of a constant temperature and fast linear heating of the samples in the resonator to a specified temperature.

The optical diffuse reflection spectra in the visible region were recorded on a Specord M-40 spectrophotometer in flat quartz cells ~20 mm in diameter. The powders were poured as ~7-mm thick layers and compacted under a pressure of ~0.1 kg cm^{-2}.

Mass spectra were recorded on an MKh-1306 instrument (EI, 70 eV). Solid samples were introduced using the built-in standard admission system. The samples were heated to 200 °C.

The reaction fronts in the SHS were stopped (quenched) by fast cooling of the reacting samples by liquid nitrogen.

The local X-ray spectral analysis (LXSA) was carried out on an ISXA-733 X-ray microanalyzer (Jeol, Japan). To protect the samples from destruction,[21] measurements were carried out at the minimum radiation power. The diameter of the electron probe was <2 μm. The local elemental compositions in various phases were determined using the CMZAFM program. The contrast in the photomicrographs obtained in the "compo" mode is due to the different average atomic numbers in the phases.[22] The polished sections were prepared by dry polishing at a low speed of the wheel. To ensure that the polished samples be mechanically strong, the pressure of mix pressing was increased to 30 kg cm^{-2}. Electrical conduction of the polished sections was ensured by vacuum deposition of a layer of metallic copper.

Results and Discussion

Macrokinetics of the SHS process. In order to elucidate the possibility of inducing SHS and to determine its modes, comprehensive thermal analysis of the reaction was carried out by calorimetry.[23] The DTA curves of the components exhibit endothermal peaks due to melting of HQ at 74 °C (Fig. 1, curve *1*)[16,17] and CA at 158 °C (Fig. 1, curve *4*) and an exothermal peak for CA decomposition at 198 °C (see Fig. 1, curve *4*) (*cf.* Ref. 24). During linear heating, the reactant mixtures undergo an exothermal reaction (see Fig. 1, curves *2* and *3*), which occurs far ahead of the CA decomposition. About 10% of the total heat is slowly evolved up to 57 °C, and then the remaining heat is evolved rapidly.

The fact that the extreme temperature of the exothermal peak displayed by the mixture (72 °C) is close to that of the endothermic peak for HQ melting (see. Fig. 1, curves *1* and *2*) suggests a liquid-phase mechanism of the reaction between the powders, so that the reaction is accompanied by melting of the HQ crystals. This is indicated by the absence of mass loss directly during the exothermal reaction (Fig. 1, curve *5*).

The heat of the reaction is 129±9 and 168±9 kJ mol^{-1}, for n = 1 and 2, respectively, *i.e.*, it increases 1.3-fold as

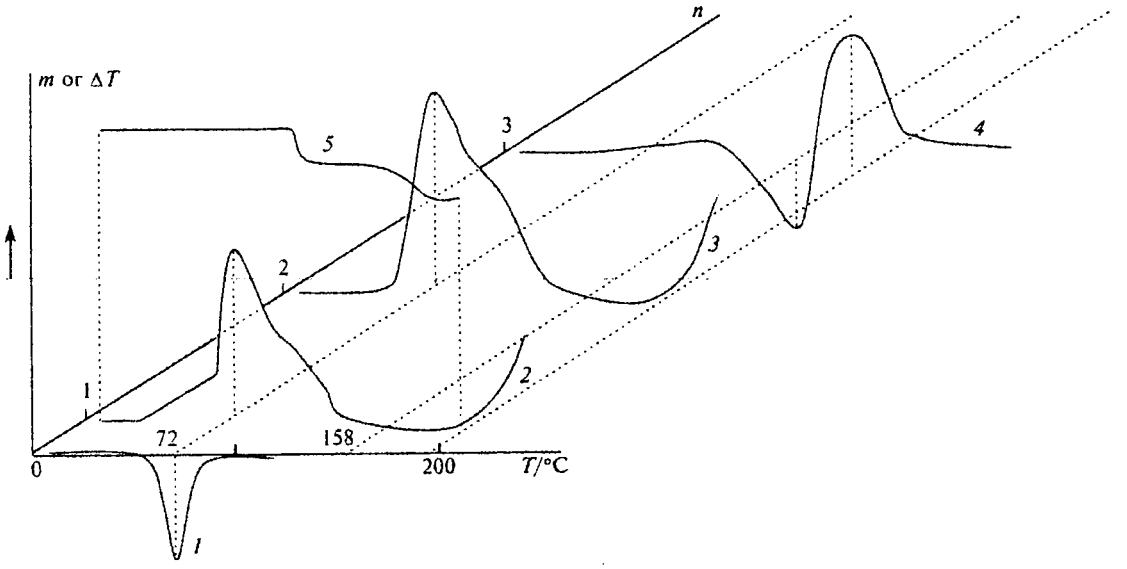

Fig. 1. Derivatogram of the HQ—CA system: (*1*—*4*) DTA curves ((*1*) HQ; (*2*) and (*3*) mixtures with n = 1 (*2*) and 2 (*3*); (*4*) CA); (*5*) TGA curve; n = [CA] : [HQ].

n increases 2-fold, indicating that the stoichiometric coefficient of the exothermal reaction is $1 \leq k \ll 2$.

Substantial mass loss is detected only after heat evolution at $T \approx 100$ °C has been completed (see Fig. 1, curve *5*), when the reactants do not undergo thermolysis. This suggests that the mass loss might be due to the evolution of water vapor. The amount of water evolved is 1 mole per mole of HQ or CA. Apparently, the same amount of water is lost upon the subsequent heating of the mixture to 200 °C.

An autowave mode is readily initiated in macroscopic amounts (>3 g) of the reactant mixture by a thermal pulse equal to ~150 J at a temperature of ≥70 °C, which is determined with allowance for the DTA data.

Figure 2 shows photographs of the reacting sample taken in reflected light. The reaction is not accompanied by luminescence in the visible region of the spectrum, which occurs in inorganic systems at high temperatures. However, the initial mixture and the products are colored differently in the reflected light (white and dark green, respectively). Therefore, the initial mix and the final product separated by the reaction front can be distinguished in the sample by sight.

The initiation area has a diameter of ~5 mm. The front arises in this area as a hemisphere and, while propagating over the blend, it becomes even and reaches the opposite side of the sample as a curved plane on whose surface fractal projections with sizes of the order of the particle size can be clearly seen. A liquid phase is formed in the front. After the wave has passed, dendrite-like crystals appear in the sample. The SHS in this particular case is distinguishable by sight from that in samples with smaller diameters.[11]

A typical temperature profile of the synthesis wave is a smooth curve without isothermal flattened sections or inflection points, which is characteristic of one-stage thermal processes (Fig. 3, curve *1*). Differentiation of this curve (Fig. 3, curve *2*) makes it possible to estimate the initiation temperature $T^* = 58$ °C,[3,11] which is in good agreement with the DTA data.

The low values for the maximum temperature in the front (T_{max}) and for the synthesis wave velocity (u) (Fig. 4), typical of organic systems,[1,2] are due to relatively low melting points and heats of reactions of molecular organic crystals.[8–10] At any n, the T_{max} value is lower than the melting point of CA but greater than that for HQ, pointing to the mechanism of capillary spreading of HQ.[3]

In the plot for the variation of T_{max} as a function of u constructued in the $\ln(u/T_{max})-1/T_{max}$ coordinates (see Fig. 4, curve *3*),[1,25] two linear sections can be distinguished, $-0.5 \leq n \leq 1$ at 100° C $\leq T \leq 115$ °C and $1 < n \leq 2$ at 115 °C $< T \leq 140$ °C (correlation coefficient 0.995). They correspond to two modes of interaction at different n: low-temperature ($n \leq 1$) and high-temperature ($n > 1$) (see Fig. 4, curve *3*). The effective activation energies (E_a) for these modes, estimated under the

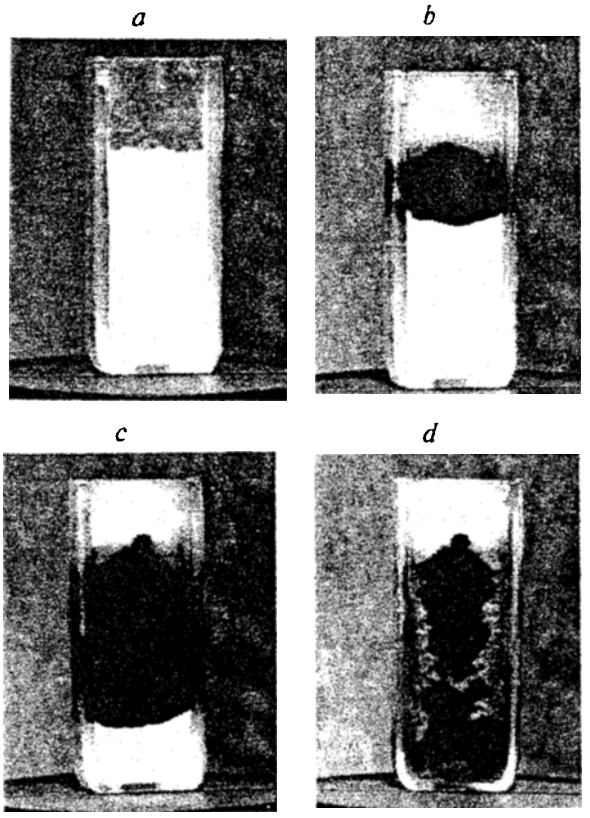

Fig. 2. Photographs of the reaction mixture of HQ and CA: (*a*) the initial mixture, (*b*) initiation of SHS, (*c*) propagation of the SHS front, (*d*) cooling of the burnt sample.

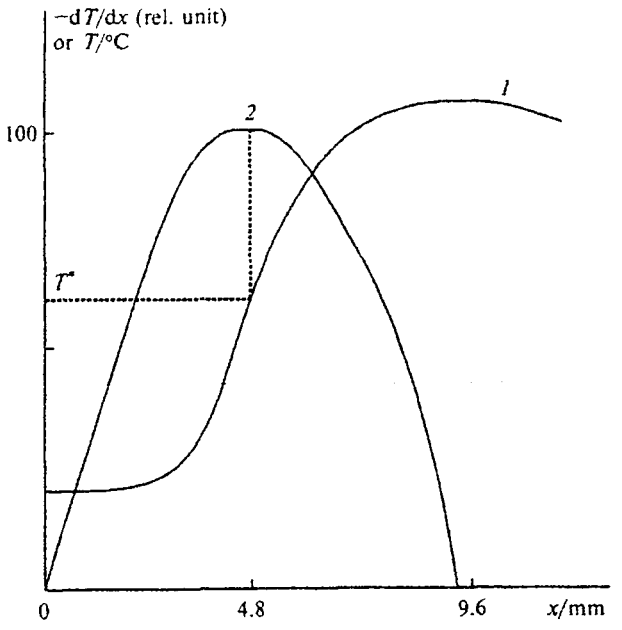

Fig. 3. Temperature profile of the wave of the reaction of HQ and CA: T (*1*) and $-dT/dx$ (*2*); x is the linear coordinate along which the reaction wave propagates.

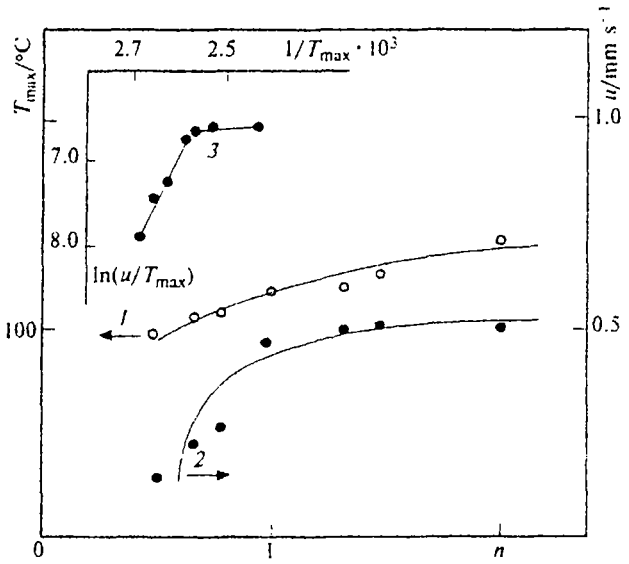

Fig. 4. Dependence of T_{max} (*1*) and u (*2*) on the mixture composition (n = [CA] : [HQ]) and T_{max} on u in the $\ln(u/T_{max})$ and $1/T_{max}$ coordinates (3).

assumption of one-stage first-order reaction without gas evolution (elementary combustion model of the Ist kind[26]), are 42 and 0.4 kcal mol^{-1}.

Calculation of the combustion parameters allows one to characterize these modes.[27–29] For $n = 1$, the experimental values are $T_0 = 293$ K, $T_{max} = 388$ K, $E = 42$ kcal mol^{-1}. It follows from the calculated values, $\beta = RT_{max}/E = 0.0183$, $\gamma = \beta T_{max}/(T_{max} - T_0) = 0.0747$, and $9.1\gamma - 2.5\beta = 0.635$, that in this case, nondegenerate stable combustion is observed. When $2 > n > 1$, $T_0 = 293$ K, $T_{max} = 413$ K, and $E = 0.4$ kcal mol^{-1}. The calculated values $\beta = 2.049$, $\gamma = 7.052$, and $9.1\gamma - 2.5\beta = 59.051$ show that at $n > 1$, the combustion mode actually changes to combustion with phase transition (elementary model of the IInd kind[26]), in which T_{max} is determined by the boiling point of water.

The break point separating these modes is located at $n = 1$, which may correspond to a stoichiometric coefficient k of the exothermal reaction equal to 1. Below $n = 0.5$, the autowave reaction does not occur at all since the blend is highly diluted by an excess of the reducing agent, HQ. The HQ molecules are fairly stable to heating; therefore, in the $0.5 \le n \le 1$ range, excess HQ is not involved in the reaction and acts as an inert diluting agent. Thus, only the main activated exothermal reaction with $k = 1$ occurs.

Excess oxidant CA ($n > 1$) brings about secondary exothermal processes. Nonactivated reaction occurs; the reaction temperature exceeds 100 °C, which causes evaporation of the water formed (elementary model of combustion of the IInd kind[26,29]) and may even cause ejection of the product, which looks like a dark-brown sintered porous material, out of the vessel. Water evaporation in the SHS front stabilizes the combustion temperature near 100 °C. The condensation of water vapor, which is filtered through the porous mix ahead of the reaction front, creates conditions for the process to occur in a thin layer of water (degenerate mode, $\gamma > 0.125$). The measured E_a value refers to boiling of water, which can be induced by either an increase in the heat content of the mix or a decrease in the heat loss (for example, due to higher initial temperature, a greater sample diameter, *etc.*).

During the reaction at $n = 1$, substantial (up to 40%) shrinkage of the mix occurs. The resulting cast reaction product remains plastic for some period because it contains a substantial amount of water, which is detected as drops of the condensate on the cold walls of the beaker. The loss of weight due to the water evaporation during combustion does not exceed several weight percent. After crystallization, the reaction product has a dark green color, which changes to green-yellow upon grinding and drying over $CaCl_2$.

It is known[3–6] that mobile phases, even present in small amounts, have a substantial effect on the combustion macrokinetics. In our case, the partial evaporation of the water formed in the reaction maintains a T_{max} of about 100 °C at $n \le 1$ and thus prevents thermolysis of yet unreacted CA. Meanwhile, while moving and, possibly, condensing in the sample, water vapor influences the heat and mass exchange processes and the rate of the chemical reaction between the reactants both inside and outside the synthesis wave.

To verify the latter assumption, the effect of solvent admixtures on the process macrokinetics was studied. This was done by comparing the u and T_{max} values for samples prepared by drying the powders to a certain initial state and then keeeping them in the vapors of various solvents. Water and protic and aprotic pure organic solvents (hydrocarbons, alcohols, ketones, halocarbons, *etc.*), with various polarities and molecule sizes, were used as additives; these compounds can get into initial powders during their manufacture, processing, and storage. A substantial increase in T_{max} (to 190 °C) and u (to 1 mm s^{-1}) after drying the powders was found (*cf.* Fig. 3). After adsorption of solvents or water, the low u (0.55±0.09 mm s^{-1}) and T_{max} (130±5 °C) parameters were restored; the values depended on the nature of the solvent used.

These results account for the changes in u and T_{max} observed on increasing n from 1 to 2, when a substantial amount of water forms upon dehydration of excess CA at the reaction temperature, as well as for the poor reproducibility of the u and T_{max} values found for different batches of the reactants.

The reaction studied clearly demonstrates a general feature of organic SHS processes, namely, the easy variability of macrokinetic parameters upon minor changes of various factors (for instance, n or the purity of the powders). This, in turn, reflects the variability of the chemical composition of SHS products,[3] which is due to multiple functionality and low thermal stability of organic compounds.

Analysis of the reaction products. The chemistry of the process. Chloramine B can exhibit both oxidative and chlorinating properties, as follows from the formal scheme of its decomposition[15] (Scheme 1).

Scheme 1

$$PhSO_2NNaCl \cdot 3H_2O \longrightarrow PhSO_2NH_2 + NaOCl + 2\,H_2O$$

$$NaOCl \longrightarrow NaCl + [O]$$

$$NaOCl + 1/2\,H_2O \longrightarrow NaOH + [Cl] + 1/2\,[O]$$

Therefore, with allowance for the chemical properties of HQ,[16,17,19,30] it can be suggested that the products of SHS can include hydroxy and chloro derivatives of HQ, in addition to the compounds presented in Scheme 1 (benzenesulfonamide, NaCl, NaOH, water).

CA does not undergo thermolysis during SHS according to Scheme 1 because the temperature of decomposition of CA (198 °C, see Fig. 1, *cf.* Ref. 22) is much higher than the maximum temperature of the process (100—115 °C). This is also indicated by the fact that autowave decomposition cannot be induced in the initial CA, apparently, because this reaction is endothermic.

Attention was centered on the analysis of the SHS products obtained in a mixture with a [CA] : [HQ] molar ratio (n) equal to 1, which ensures, as shown above, complete conversion of the reactants.

The loss of sample weight immediately after the SHS does not exceed 0.56%. Thus, virtually no gaseous products are formed during SHS. Dehydration of the SHS product ($CaCl_2$, 30 °C, 24 h) results in the loss of 1.08 moles of water per mole of HQ taken. Thus, the elemental composition of the solid reaction product can be calculated with the knowledge of the elemental composition of the mix, $C_{15}H_{15.8}N_2O_{4.9}SNaCl$.

Annealing (350 °C) of the product in air affords a white dry residue; its calculated molecular weight is 65 (a mixture of NaCl, NaOH, and Na_2CO_3), indicating the presence of volatile organic products of SHS and the absence of carbon black or resin formation.

A saturated (0.4%) aqueous solution of the SHS product shows an alkaline reaction. Titration of this product reveals the presence of 0.86 moles of a 1 N alkali per mole of HQ taken.

The heaviest ions in the mass spectra of the SHS product are responsible for peaks with m/z 178—180, which can be matched by the species $C_9H_7NO \cdot H_2O_2$ or C_9H_5NOCl. Benzenesulfonamide (m/z (I_{rel} (%)): 156 (44) $[M - H]^+$, 141 (33) $[PhSO_2]^+$, 77 (33) $[Ph]^+$) and hydroquinoline (m/z (I_{rel} (%)): 145 $[M]^+$ (100)) were identified. The latter compound could have formed only from HQ derivatives because HQ itself is entirely consumed during SHS.

The X-ray diffraction patterns of the SHS product contain reflections corresponding to NaCl and benzenesulfonamide phases (Fig. 5, *d*,*e*); in mixtures with $n < 1$, HQ was also identified (see Fig. 5, *c*). The amplitude of the reflections due to the latter product decreases with an increase in n and becomes zero when $n = 1$. During drying of the SHS product, the reflection amplitudes in the X-ray diffraction patterns increase, which is associated with crystallization of the resulting water-soluble substances (see Fig. 5, *d*,*e*).

When $n > 1$, reflections due to NaCl predominate (see Fig. 5, *f*,*g*) because organic reaction products are partially evaporated and thermolyzed, yielding an alloy amorphous to X-rays. The similarity of X-ray diffraction patterns obtained at $n \geq 1$ indicates that at the n values studied, the same reaction occurs. Complete assignment of the reflections is impossible because no data on the phase diagrams of the hypothesized SHS products are available.

The ^1H NMR spectra of the SHS product exhibit signals for almost all the protons present in the aromatic rings of HQ and CA in the region of δ = 6.7—8.4 (Fig. 6, curves *1* and *2*) and no signals of acidic or nonaromatic protons (δ = 9—12 and 2—5, respectively[31]) (see Fig. 6, curve *4*). Hence, the aromatic rings are not cleaved during the reaction. Due to fast proton exchange, the signals of the OH and NH_2 groups (δ = 4.5—5.1) are not resolved. It can also be suggested that the H(2) ($\delta \approx 8.1$) and H(4) ($\delta \approx 8.7$) atoms[31,32] in the HQ molecule are not affected by SHS because their signals do not disappear from the spectra but are only

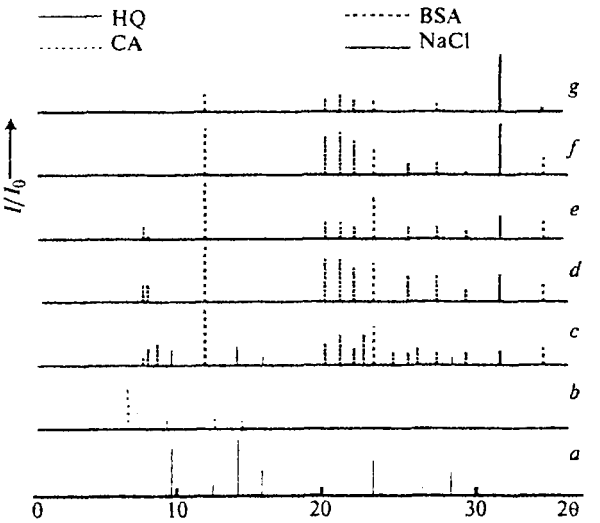

Fig. 5. X-ray diffraction patterns of the HQ—CA system: HQ (*a*); CA (*b*); n = 0.5 (*c*); n = 1, immediately after the synthesis (*d*); n = 1, after drying (*e*); n = 2 (*f*), 3 (*g*); Cu-Kα radiation; peaks with intensities lower than 30% are not shown; the amplitude of the maximum peak is 1. Thin lines correspond to HQ, the bold line shows NaCl, the dashed line is CA, and dash-and-dot lines correspond to BSA.

broadened (*cf.* Fig. 6, curves *1*, *3*—*5*). This can be explained by spin density redistribution in the rings due to the appearance of substituents (O, Cl) in other positions of the HQ molecule and formation of intramolecular hydrogen bonds. As n increases from 0.5 to 1, the signals of the HQ protons gradually become less intense and finally disappear (see Fig. 6, curves *3*—*5*), as has been observed in the X-ray diffraction patterns.

The IR spectra of the dried SHS product (Fig. 7, curve *4*) allow reliable identification of the NH_2 (a doublet at 3330 and 3240 cm^{-1} and a band at 1560 cm^{-1}) and SO_2 (1170 and 1380 cm^{-1}) groups of benzenesulfonamide.[31] The decrease in the intensity of the broad band of the hydrogen-bonded OH groups (3400—3200 cm^{-1}) and the disappearance of the band of single OH groups (3590 cm^{-1})[31] after the SHS is due to the consumption of the water of crystallization of CA during the reaction (*cf.* Fig. 7, curves *2* and *4*).

The increase in n from 0.5 to 1 (see Fig. 7, curves *3* and *4*) is accompanied by changes similar to those described above in relation to the X-ray diffraction and ^1H NMR data (see Figs. 5 and 6). This is manifested as weakening of the nonoverlapping absorption bands of the reactants (3590 and 1260 cm^{-1} for CA and 1290 and 1280 cm^{-1} for HQ) and strengthening of the bands of products (1560 cm^{-1}). The characteristic absorption band at ~1330 cm^{-1} that appeared after the reaction (see Fig. 7, curve *4*) can be due to vibrations of the N→O group[31,33] in 8-hydroxyquinoline *N*-oxide or its hydrate. The formation of this product appears quite likely in view of the ability of HQ to undergo exothermic oxidation.[16,17,19]

The absorption bands at 28000 cm^{-1} and 18800 cm^{-1}, due to the aromatic rings in HQ,[34] do not disappear from the diffuse reflection spectra of the SHS products (*cf.* Fig. 8, curves *2* and *3*). Therefore, it can be claimed that the interaction occurs without destruction of the aromatic rings of HQ.

The bands that appear at 13500 cm^{-1} and 23500 cm^{-1} (see Fig. 8, curve *3*) may be due to 8-hydroxyquinoline *N*-oxide or its crystal hydrate; the former band corresponds[35] to the $n \rightarrow \pi^*$ transition.

The removal of water from the freshly prepared SHS product during storage in air or drying is accompanied by a smooth increase in the total extent of reflected light (*cf.* Fig. 8, curves *3* and *4*). This is due to product crystallization, which still goes on after the synthesis and during the product drying. This process, which is also detectable in the X-ray diffraction patterns (see Fig. 5,

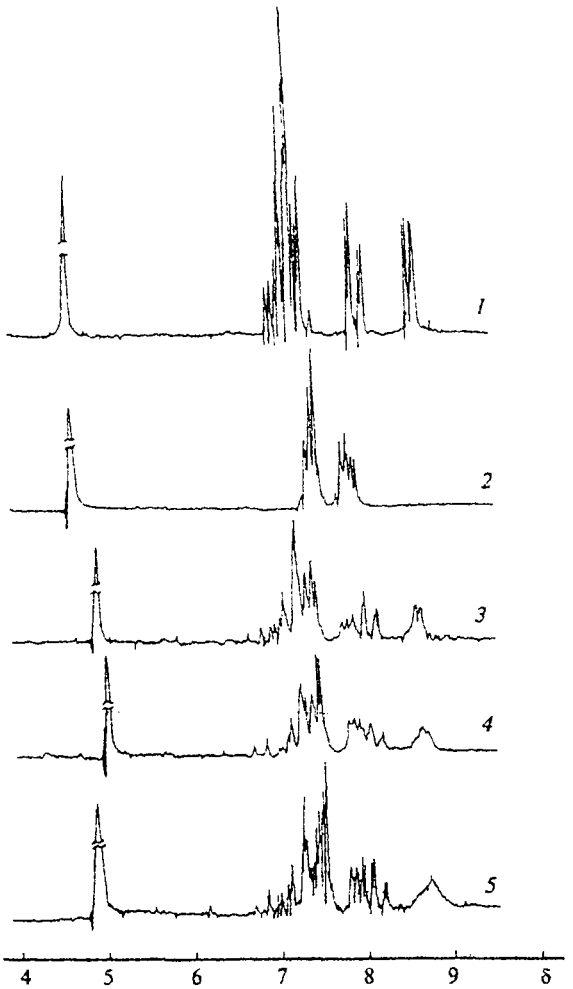

Fig. 6. ^1H NMR spectra of the HQ—CA system: HQ (*1*); CA (*2*); n = 0.25 (*3*), 0.5 (*4*), 1 (*5*).

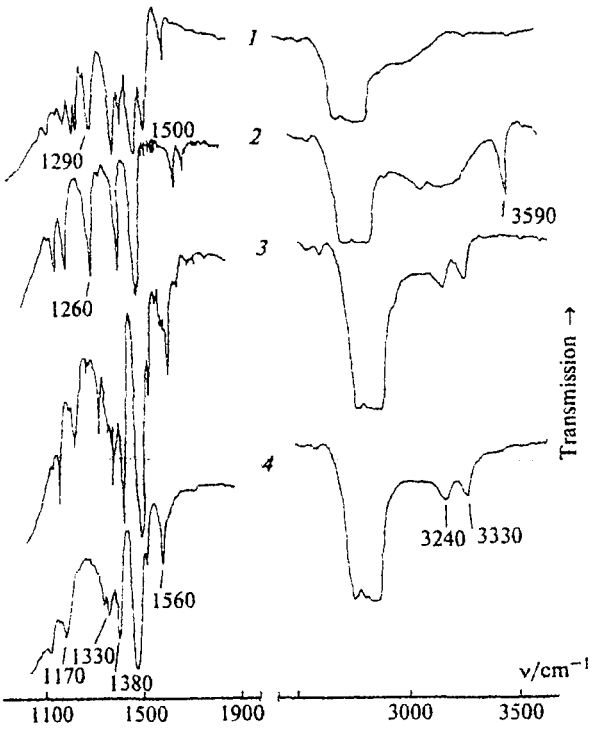

Fig. 7. IR spectra of the HQ—CA system: HQ (*1*); CA (*2*); n = 0.5 (*3*), 1 (*4*).

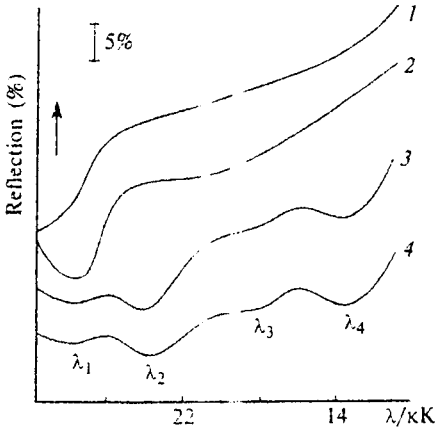

Fig. 8. Diffuse reflection spectra of the HQ—CA system: CA (*1*); HQ (*2*); dried SHS product (*3*); the SHS product immediately after the synthesis (*4*).

d,e), results in a greater or lesser reflecting surface area of the samples.

N-Oxides are normally paramagnetic[35] and chloramines tend to undergo chain radical processes[36]; therefore, the ESR spectra of the products were studied. A sample dried after SHS was found to be responsible for a symmetrical singlet ($g = 2.0043 \pm 0.0009$, $\Delta H = 10.6$ G), which coincides with the signal of the reference sample of the *N*-oxide. The parameters of the singlet remain virtually unchanged after the sample has been evacuated, cooled to 77 K, heated to 335 K, and recrystallized from EtOH. Such a behavior is consistent with representation of the *N*-oxide molecule as a free radical, in which the spin density of the unpaired electron is mainly concentrated on the N→O bond.[35]

After a freshly prepared sample has been dehydrated at room temperature, the spin concentration increases to 10^{19}—10^{20} spin g^{-1} (a 0.8—8.0% content of the paramagnetic substance). The actual content of the *N*-oxide in the samples is greater because it is present as the monohydrate, which has no paramagnetic properties; hence, the spectrometer detects only those molecules that form upon partial dehydration of the hydrate according to Scheme 2.

Scheme 2

$$C_9H_7NO_2 \cdot H_2O \rightleftharpoons C_9H_7NO_2 + H_2O$$

The chemical binding of the *N*-oxide to a water molecule results in delocalization of the spin density of the N→O bond, enhancement of exchange processes, and, as a rule, in a decrease or even vanishing of the ESR signal.[35] This was observed in freshly prepared products, in those recrystallized from ethanol, and in solutions of the SHS products (in ethanol or DMSO), in which the hydrate dissociates[37] by Scheme 3.

Scheme 3

$$C_9H_7NO_2 \cdot H_2O \rightleftharpoons [C_9H_7NO_2 \cdot H]^+ + OH^-$$

After removal of the solvent, the initial content of spins in the SHS products is restored.

The chromatograms of the SHS product show the presence of two groups of organic compounds; $R_f = 0.1$ might correspond to benzenesulfonamide (BSA) and $R_f = 0.87$ is assumed to correspond to hydroxyquinoline derivatives.

The dried SHS product was found to contain chlorine in an amount close to the calculated amount (9.30%); 2.36% is represented by Cl^- (NaCl, which is produced by Scheme 1 in a quantity of 3.7% or 0.26 moles). Since CA and HQ are completely consumed in the SHS, the HQ molecule is not destroyed, and no polychlorinated derivatives of HQ are formed (see above), the rest of the chlorine (6.94%) occurs as a monohalogenated HQ.

The results of elemental analysis of dry residues from the extracts of the SHS product into solvents (water, ethanol, ether) also point to the presence of a substantial amount of chlorine (10.46—13.52%) and sulfur (7.62—8.56%). The calculated ratio of elements (C, H, O, N, Cl, S) in the dry residues does not correspond to an individual compound. This suggests that the extractable compounds are stable BSA complexes with the products of transformation of HQ.

Thus, the whole set of analytical data shows that in the SHS the degree of conversion of an equimolar mixture of HQ and CA powders is 100%. The solid product formed in the SHS contains NaCl (3.7%), NaOH (8.7%), water (4.7%), benzenesulfonamide (38.1%), monochlorinated HQ (33.5%), and the HQ *N*-oxide hydrate (0.8—8.0%). These estimates are rough because of the error in the double integration of the ESR spectra and the uncertainty in the determination of the degree of dissociation of the *N*-oxide hydrate by Schemes 3 and 4. Therefore, the formation of other hydroxy and chloro derivatives of HQ, benzenesulfonamide, or their complexes in 3—6% yields also cannot be ruled out. The results obtained suggest that the reaction proceeds by Scheme 4.

Scheme 4

$$C_9H_7NO + PhSO_2NNaCl \cdot 3H_2O \longrightarrow \begin{cases} C_9H_7NO_2 \cdot H_2O + PhSO_2NH_2 + NaCl + H_2O \\ C_9H_6NOCl + PhSO_2NH_2 + NaOH + 2H_2O \end{cases}$$

It has been shown previously[11] that the SHS in the mixture studied is a one-stage thermal process, which starts with melting of HQ, and that the wave in the

reaction area is completed over 5—7 s. In addition, as shown above, thermolysis and hydrolysis of CA, which could account for a multistage SHS, are not involved in the process. Therefore, a reaction mechanism assuming synchronous interaction between the initial molecules and formation of the final products with participation of the CA water protons and the lone electron pair of the HQ nitrogen appears probable (Scheme 5).

Scheme 5

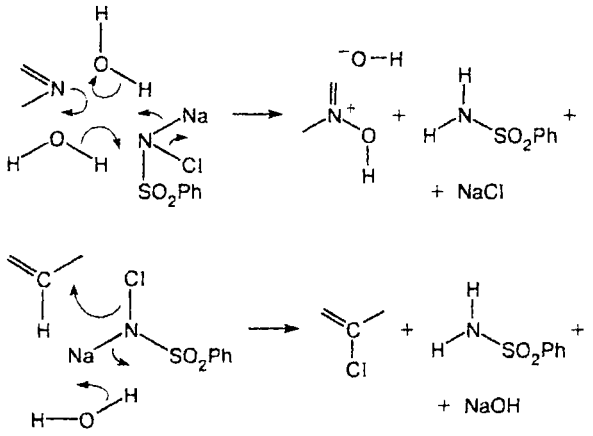

The mechanism of solid-phase interaction. A short-term storage of a mixture of HQ and CA powders at room temperature changes its color, texture, and ability to undergo SHS. Previously,[7] a similar situation has been observed for mixtures of piperazine with malonic acid and has been explained by assuming that the reaction occurs at the contact points between the particles.

Study of this interaction, below referred to as solid-phase reaction, at room temperature presents interest because its rate substantially increases at the SHS temperature and it starts to play a noticeable role, especially in the area of heating of the SHS wave.[3—5]

Below we present the results of a study of the solid-phase reaction performed using ESR, optical diffusion reflectance spectroscopy, and powder X-ray diffraction analysis.

The ESR spectra of the initial HQ exhibit a signal for the HQ *N*-oxide with a concentration of ~10^{17} spin g^{-1} (~0.01% of the substance).[11] In a freshly prepared mixture of the reactants with n = 1, the intensity of this signal increases 3—5-fold over a period of several minutes (Fig. 9, region I); then, over a period of several days, it increases 2—3-fold according to a linear pattern (correlation coefficient 0.98) (see Fig. 9, region II). Subsequently the growth of the signal virtually stops (see Fig. 9, region III). Such a stepwise dependence attests to a multistage process. The first step is a fast surface reaction at the interparticle contact points. This is confirmed by the strong relationship between the rate of the process and the compacting pressure: as the pressure increases from 0.3 kg cm^{-2} to 25 kg cm^{-2}, the rate of the first stage increases 3—4-fold due to the increase in the contact area of the particles.[38] The rate of the second stage is determined by the diffusion of the reactants toward the reaction surface.

In the optical diffuse reflectance spectrum of a freshly prepared mixture with n = 1 (Fig. 10, curve *3*), absorption bands (see Fig. 10, curves *4* and *6*) characteristic of the SHS product (see Fig. 10, curve *7*) appear after some period. Their intensity gradually increases, so that in the limiting case, the spectrum of the mixture coincides qualitatively with that of the SHS product (*cf.* Fig. 10, curves *6* and *7*). Apparently, the chemical reaction occurring in this case is the same as in the SHS.

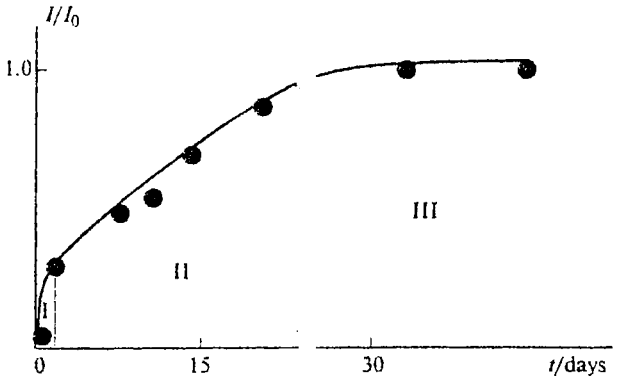

Fig. 9. Kinetics of the solid-phase reaction based on ESR data.

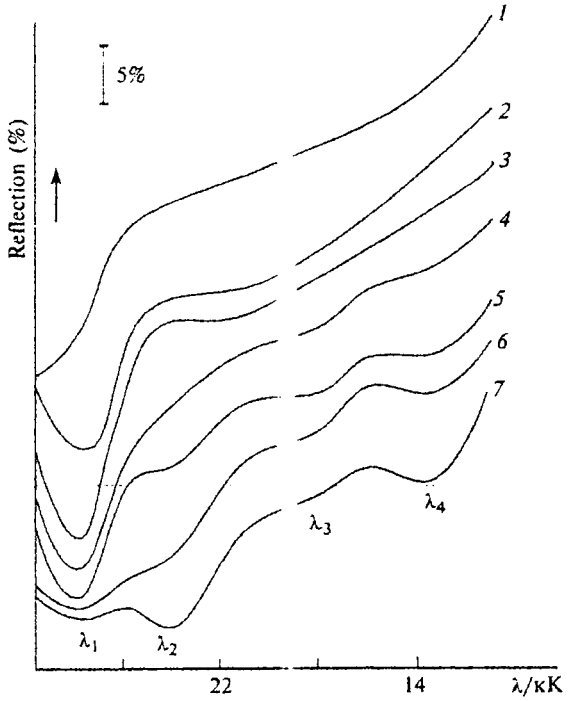

Fig. 10. Diffuse reflection spectra: CA (*1*); HQ (*2*); mixtures of HQ and CA powders with n = 1 (*3—6*): immediately after mixing (*3*), 24 h later (*4*), after trituration (*5*), 5 days later (*6*); the SHS product (*7*).

The rate of the linear increase in the intensity of the band referring to the aromatic ring of HQ (λ_1 = 28000 cm^{-1}, see Fig. 10, curve *2*), which is determined from the slope of the straight line (Fig. 11, straight line *1*), is the lowest among those observed. The increase in the amplitude of this band is due to the decrease in the total reflecting capacity of samples rather than to chemical transformations.

The rates of the growth of the bands with λ_3 = 18800 cm^{-1} and λ_4 = 13500 cm^{-1} (see Fig. 11, curves *3* and *4*) are identical and are higher than that for λ_1. Apparently, these bands are due to a chemical transformation and belong to the same product. The kinetic curve for the band λ_2 = 23500 cm^{-1} (see Fig. 11, curve *2*) does not coincide with those for other bands but it has a linear section parallel to the curves for λ_3 and λ_4 (see Fig. 11, curves *3* and *4*). This implies synchronous formation of all the colored products. A similar linear section can be found by ESR (see Fig. 9). The rate of the increase in the amplitude of the bands, like that of the ESR signals, increases with the compacting pressure.

The products formed in the solid-phase reaction are deposited as a crust on the surface of the reactant particles, while the unreacted component remains inside the particles. This is confirmed by the fact that the spectrum of a triturated, partially reacted mixture (see Fig. 10, curve *6*) shows a substantial weakening of the absorption bands of the products with a simultaneous increase in the total intensity of the reflected light (see Fig. 10, curve *5*); the reactivity of the mix thus is restored. The latter is due to the renewal of the reactive surface of the particles upon the destruction of the product crust and to the decrease in the relative surface concentration of the products. The subsequent dynamics of the absorption spectra of this mixture coincides qualitatively with the dynamics of the spectra of a freshly prepared mixture.

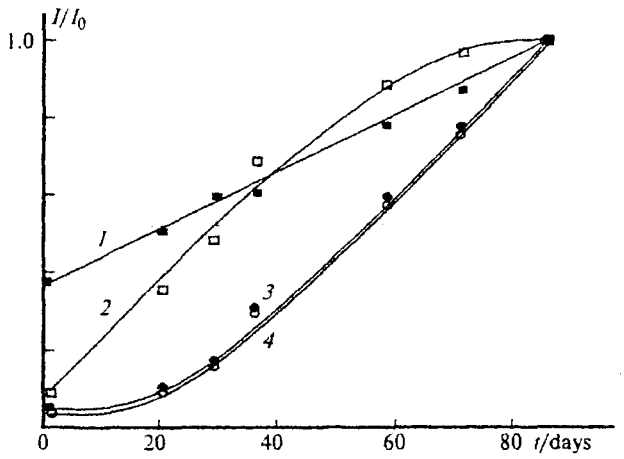

Fig. 11. Kinetics of the solid-phase reaction based on the data of optical spectroscopy: bands with λ_1 = 28000 cm^{-1} (*1*), λ_2 = 23500 cm^{-1} (*2*), λ_3 = 18800 cm^{-1} (*3*), λ_4 = 13500 cm^{-1} (*4*).

The IR spectra of a mixture in which the solid-phase reaction occurs are superpositions of the spectra of CA, HQ, and the SHS product (see Fig. 7), which confirms the similarity of this process and the SHS. The difference is the appearance of absorption bands due to hydrogen-bonded and single OH groups (3200—3400 and 3590 cm^{-1}),[31] which are typical of CA (see Fig. 7). This is due to the fact that dehydration or dehydroxylation of samples does not occur at room temperature but does occur at the SHS temperature.

To study the transformations of the crystalline phases during the solid-phase reaction, X-ray diffraction patterns of the pressed mixtures were recorded at intervals. The kinetic curves for the relative amplitudes of sets of reflections corresponding to the same substances (HQ and CA, NaCl and BSA) are located in areas marked by the same hatching in Fig. 12. These areas are rather wide and the shapes of the upper and lower borders of the areas of reactants (see Fig. 12, *a* and *b*) do not coincide. This may be due to unequal rates of the formation or destruction of the crystallographic planes with different indices, which possess different reactivities. The substantial inhomogeneity of the powders, which is manifested as line narrowing during the reaction, and autocatalysis can also be responsible for this finding.

The crystal lattices of the reactants are destroyed at different rates during the solid-phase reaction; HQ is destroyed faster (see Fig. 12, *a*) than CA (see Fig. 12, *b*). This might be due to both dissimilar mechanisms of their interaction and to different resistances of the lattices against reaction products, in particular, water.

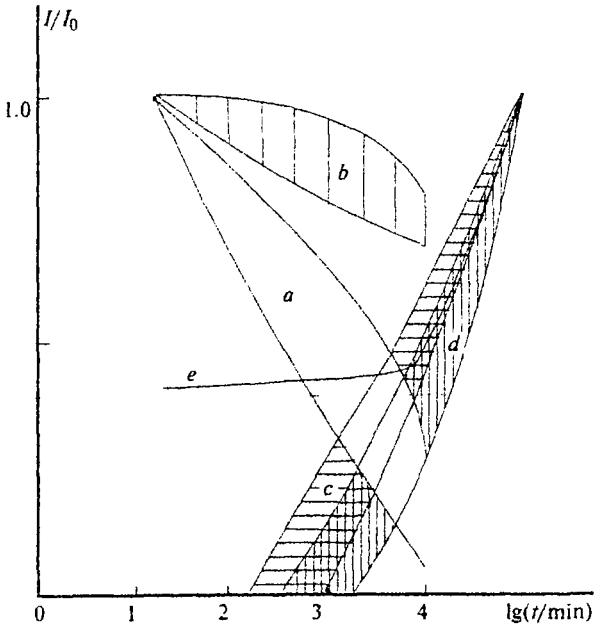

Fig. 12. Dynamics of phase transformations in the solid-phase reaction based on X-ray diffraction data: (*a*) HQ; (*b*) CA; (*c*) NaCl; (*d*) benzenesulfonamide; (*e*) the background level.

The reflections for the lattices of products, NaCl (see Fig. 12, *c*) and BSA (see Fig. 12, *d*), do not appear simultaneously with the consumption of the reactants but after a substantial delay because the process of formation of product microcrystals is hampered at room temperature. The NaCl crystals, possessing high polarity and melting point, are the first to form (see Fig. 12, *c*). The rates of the growth of reflections of both products are virtually equal, and the upper and lower borders of areas *c* and *d* are similar, pointing to synchronous formation and uniformity of the product crystals.

The chemical reaction is accompanied by an increase in the overall degree of dispersion of the mixture (amorphization) because the reactant crystals are destroyed by the nuclei of new phases. This is displayed as an increase in the background level in the X-ray diffraction patterns (see Fig. 12, *e*); the rate of this process markedly increases after the appearance of product microcrystals (autocatalysis).

Thus, the results obtained in studies of the solid-phase reaction by various methods are in good agreement with one another.

To elucidate more precisely the mechanism of the chemical transport during the solid-phase reaction between HQ and CA, samples were prepared in which the dispersed reactants (particle diameter $0.315 > d > 0.2$ mm) were not intermixed but were packed in a quartz cylindrical tube with a diameter of 8 mm as two adjacent layers, each 20-mm long (Fig. 13, *b*). Several hours later, a green-yellow ribbon appeared in the CA layer near the contact boundary. The color intensity diminished outward from the boundary. The length of the colored area Δl (Fig. 14) increased linearly with time, pointing to gas-phase reaction diffusion.[38,39]

Figure 13, *a*,*c* shows the distribution of the color centers and spins along the contact area of the layers, determined by diffuse reflection and ESR studies of parallel sections cut from the sample. The fact that these spectra are identical to those for HQ—CA mixtures and for the SHS product (*cf.* Fig. 10, curves *6* and *7*) proves that the same reaction proceeds in all cases. The fact that paramagnetic species or color centers are totally missing from the HQ layer, being present in a high concentration in the CA layer (see Fig. 13, *a*,*c*), indicates that in this case, directed transfer of only HQ molecules into the porous CA layer occurs.

To determine more precisely the mechanism of the HQ transport (surface or gas-phase diffusion), the reactant layers in the above-described samples were separated from each other by aluminum foil or by a 3-mm thick layer of quartz powder with the same degree of dispersion. In the former case no substantial changes occurred in the contact area, despite the ~0.1-mm gap between the foil strip and the wall of the tube. However, in the latter case, the situation was qualitatively the same as in the above-described experiment. This implies that HQ could be carried by gas-phase diffusion, which is consistent with the high volatility of HQ at room temperature.[16,17] Previously,[40] another possible mechanism of HQ mass transfer in the solid-phase reaction, namely surface diffusion, has been reported.

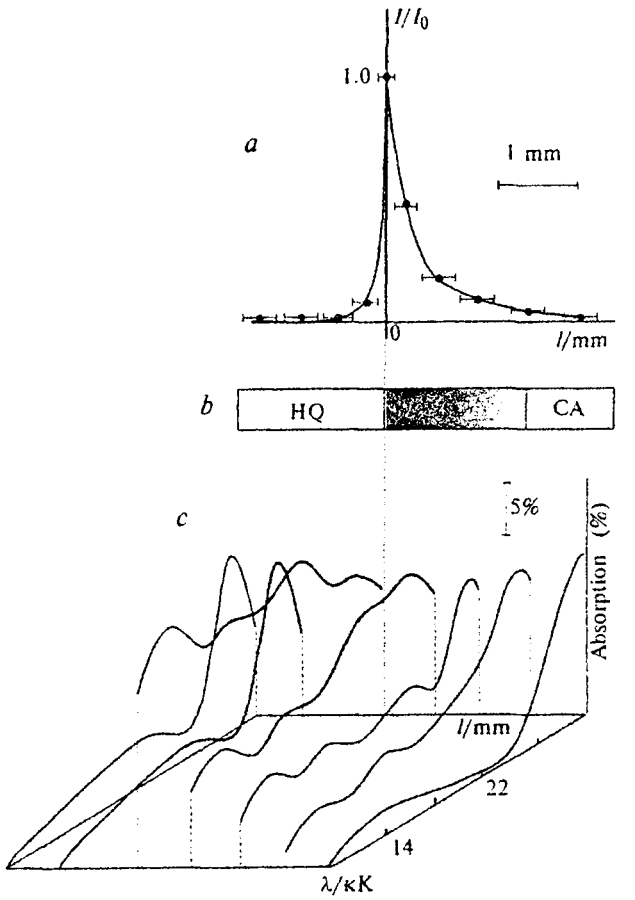

Fig. 13. Distribution of color and paramagnetic centers along the contact area of the HQ and CA layers: (*a*) relative concentrations of paramagnetic centers along the contact area; (*b*) structure of the sample; (*c*) optical spectra of sections of the contact area.

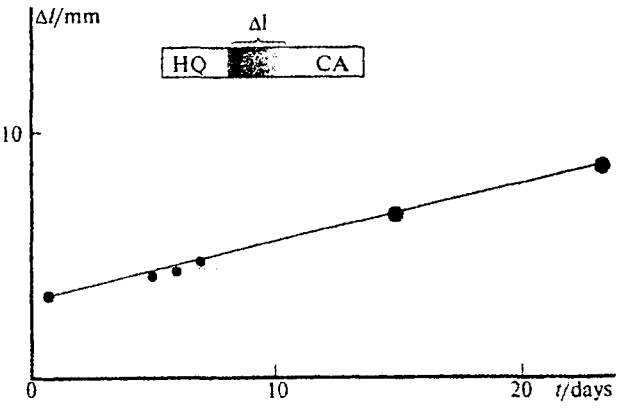

Fig. 14. Kinetics of the propagation of the colored area.

The high rate of the solid-phase reaction suggests that the reaction occurs not only due to transfer of large HQ or CA molecules through a crust of the products but also due to surface diffusion of light oxygen-containing active species (O, HO, HO_2, H_2O_2, *etc.*), capable of relay race migration, especially in the presence of water molecules[41] (Scheme 6).

Scheme 6

To verify this hypothesis, the reaction was carried out with powders subjected preliminarily to the adsorption of water or various organic solvents. Indeed, the rate of the solid-phase reaction (10 days, see Fig. 11)

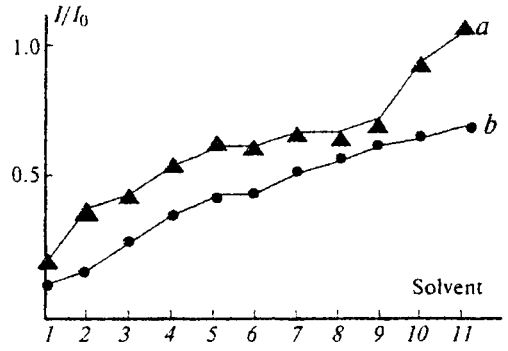

Fig. 15. Effect of adsorbed solvents on the kinetics of the solid-phase reaction: (*a*) the band with λ_2 = 23500 cm^{-1}, (*b*) the band with λ_4 = 13500 cm^{-1}. (*1*) dry mixture, (*2*) methanol, (*3*) benzene, (*4*) isopropanol, (*5*) hexane, (*6*) methyl ethyl ketone, (*7*) acetone, (*8*) chloroform, (*9*) tetrachloromethane, (*10*) ethanol, (*11*) butan-2-ol.

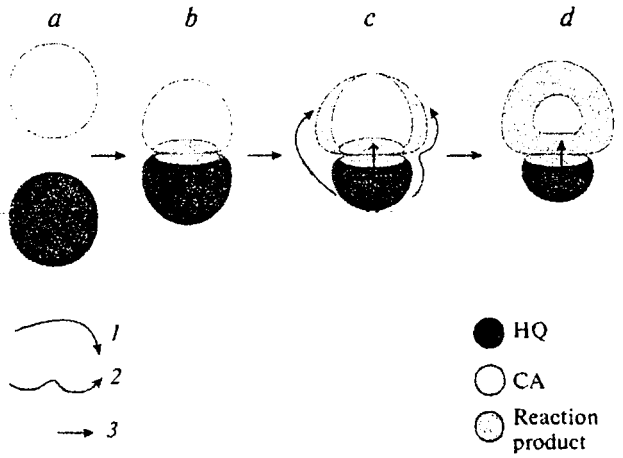

Fig. 16. Scheme of interaction of hydroxyquinoline and chloramine particles: (*1*) gas diffusion, (*2*) surface diffusion, (*3*) solid-phase diffusion.

was found to increase by a large factor (2—5-fold) after adsorption of any of the solvents (Fig. 15). A similar influence of solvent traces on the kinetics of the reaction of powders has been observed for SHS and topochemical reactions.[42]

Thus, the results obtained make it possible to propose a sequence of processes occurring in HQ and CA mixtures at room temperature and, apparently, in the heating area of the SHS wave (Fig. 16). On contacting the particles, a fast reaction occurs on the contact surface (see Fig. 16, *b*). Then, as a result of sublimation of HQ in the pores of the mixture, the surface of CA particles that does not contact directly with the HQ particles is also involved in the reaction (see Fig. 16, *c*). The loss of HQ in the gas phase is made up by its subsequent evaporation. After the CA surface has been covered by a monolayer of the reaction products, the reaction proceeds due to the surface diffusion of HQ and active species and later due to diffusion through an X-ray-amorphous layer of condensed products (see Fig. 16, *d*), in which crystals of the reaction products are formed after some period. This scheme is consistent with the mechanism of solid-phase reactions of HQ with other substances.[40]

Since the reaction in question is accompanied by change in the phase states of the reactants, it cannot be classified as a topochemical reaction.[9]

Reaction mechanism at synthesis temperatures. The next stage of the investigation included elucidation of the SHS mechanism in the 20—100 °C temperature range, which covers the temperature in the heating zone (<58 °C) and the temperature of the SHS wave initiation (≥58 °C), at which the main SHS mechanisms are realized and product formation occurs.

The ESR method provided the possibility of estimating the degree of conversion of the reactants by monitoring the formation of paramagnetic 8-hydroxyquinoline *N*-oxide molecules, $C_9H_7NO_2$ (see above and Ref. 11) according to Scheme 4.

A weighed portion of an equimolar mixture of HQ and CA was placed in a spectrometer and the ESR signal was recorded as the sample was heated to a specified temperature. The initial mix exhibits[11] a weak signal for the HQ *N*-oxide. When the temperature increases stepwise (Fig. 17, curve *1*), the amplitude of this signal increases sharply and disproportionately and reaches a maximum near the melting point of HQ (64 °C) (Fig. 17, curve *2*).

Keeping the mixture at an attained constant temperature does not bring about the expected growth of this signal. Conversely, it slightly diminishes (see. Fig. 17, curve *3*) owing to a decrease in the *Q*-factor of the resonator by the water vapor evolved. This "stepwise" kinetics of the signal growth is caused by inhomogeneity of the reactants: small or defective crystals react faster than larger ones.

When the mixture is heated to the melting point of HQ, not only the signal amplitude increases but also the

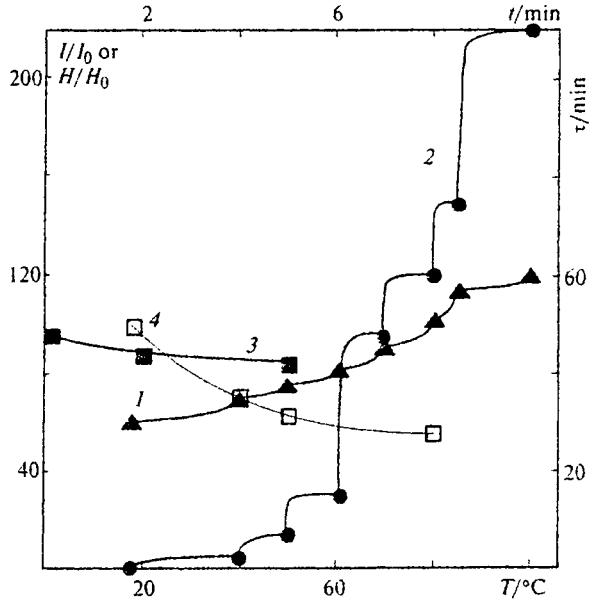

Fig. 17. Temperature and time dependences of the ESR signal: (*1*) the temperature curve $T(\tau)$; (*2*) the temperature dependence of the relative intensity $I/I_0(T)$; (*3*) the time dependence of the relative intensity $I/I_0(t)$; (*4*) the temperature dependence of the relative signal width $H/H_0(T)$; τ is the sweep time.

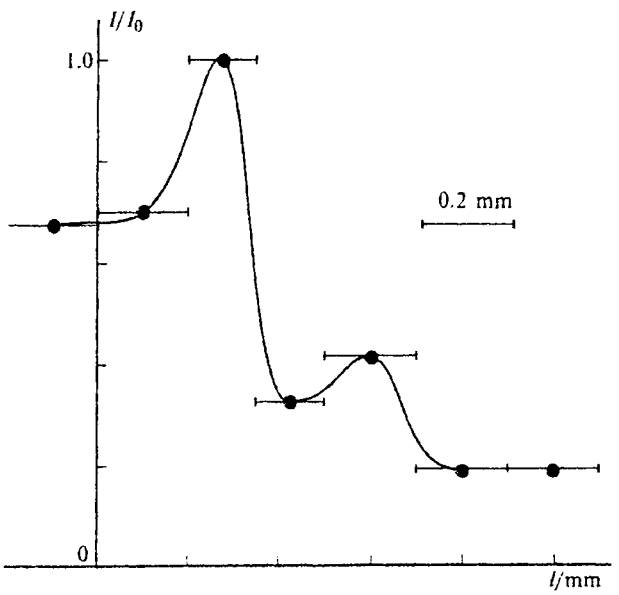

Fig. 18. Concentration profile of the front of the quenched sample.

signal markedly narrows down (see Fig. 17, curve *4*) to a ΔH value corresponding to the mixture melt. This can be due to the increase in the mobility of paramagnetic species on heating and to a decrease in their exchange interaction with the crystal lattice of HQ, which is destroyed under the influence of high temperatures.

After the melting point of the HQ crystals has been attained in the resonator, thermal explosion occurs. The water vapor thus evolved (see Scheme 4) detunes the spectrometer, which hampers further investigation of the reaction. Previously, we studied this in detail by a dynamic ESR technique, which made it possible to estimate the distribution of paramagnetic *N*-oxide molecules and the degree of conversion of the reactants in the reaction front.[11]

Additional information on the chemical processes occurring in the combustion wave of a mixture of HQ and CA was gained by investigating the microstructure and chemical composition of the surface of polished sections prepared from samples in which the SHS front had been terminated by fast cooling of the burning sample in liquid nitrogen (quenching).

Figure 18 shows the distribution of paramagnetic species along the direction of the front propagation determined by measuring their relative concentrations in a quenched sample. The sections were sliced parallel to the reaction front; the edges of the sections were set by the visually distinguishable color intensity. It can be seen that paramagnetic species are accumulated in a 0.6-mm long area, which exactly matches the reaction front. Two areas with high contents of particles were found in the front. The nonuniform distribution of paramagnetic species in the reaction front and, hence, the different degrees of transformation giving the *N*-oxide in these areas are apparently due to the oscillation mode of combustion[3] or perturbation of combustion by quenching.

Electron microscopy studies[21] of the chemical phase boundaries discloses not only the chemical structure of the surface but also the mechanism of the chemical interaction between the particles and mass transfer. Figure 19, *a* shows the picture of the longitudinal polished section of a quenched sample obtained by this method. It can be seen that the front contains three main regions, *viz.*, a porous two-phase region of the initial mix (I); a 600—800-μm region comprising at least two phases with a small number of pores, which is the transient area containing the reaction intermediates (II); and a ~300-μm relatively homogeneous, slightly porous region composed of the final reaction product (III). The white dot inclusions are corundum particles having gotten into the samples during polishing. The microstructures of these regions at a greater magnification are shown in Fig. 19, *b—d*, respectively.

Three structural components of region I are seen in the photograph of the initial mix (see Fig. 19, *b*); the solid backing is the CA phase, the broad black inclusions with a size of ~30—40 μm are the HQ phase, and the black narrow lines are cracks and pores having arisen during the sample preparation.

In the transient phase II (see Fig. 19, *c*), three microregions differing in elemental composition are distinguished. The light phase is a CA particle, the black phase is an HQ particle, and the surrounding gray phase, which

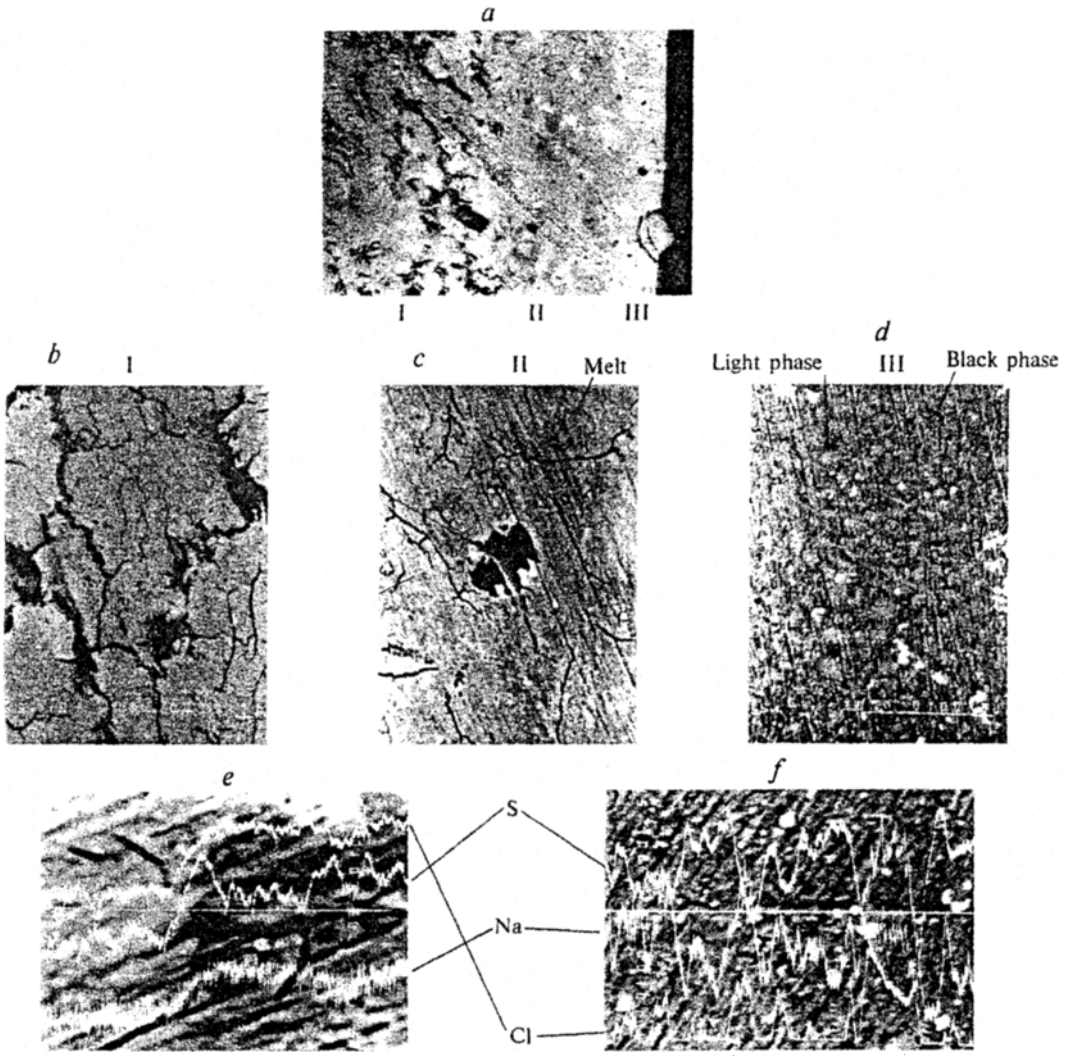

Fig. 19. Microstructure of the front of the quenched sample: (*a*) three characteristic regions of the front, ×60; (*b*) the initial mixture, region I, ×600; (*c*) the transient region II, ×540; (*d*) the final SHS product III, ×440; (*e*) concentration curves in region II, ×1000; (*f*) concentration curves in region III, ×1000, the "compo" mode.

contains Na, Cl, S, and O and is characterized by a much (1.5—2 times) greater content of C compared to that corresponding to CA, is the reaction melt of CA and HQ. Analysis of the concentration profiles of Na, Cl, and S at the CA—melt interface (see Fig. 19, *e*) demonstrates that the synchronous course of the curves for these elements in the CA particle, which is peculiar to individual substances, is disturbed in the melt area, which is due to the started destruction of the CA molecule and segregation of Cl- and S-containing substances in separate phases.

Thus, at the reaction temperature, the low-melting HQ undergoes capillary spreading in the CA phase. The pores occurring in the mix disappear (*cf.* Fig. 19, *b* and *d*); this is one of the reasons for the shrinkage of samples observed after combustion.

Region III (see Fig. 19, *d*) consists of two uniformly scattered microregions with different elemental compositions with a characteristic size of 5—10 μm, which are referred to below as "light" phase (with a greater average atomic number) and "dark" phase (with a smaller average atomic number). Qualitative local X-ray spectral analysis (LXSA) showed the presence of the same elements (Na, Cl, C, N, S, O) as in CA. The main difference between these microregions is the difference in the proportions of S, Na, and Cl. In the "light" phase, Na and Cl predominate, while S predominates in the "dark" phase. This is clearly demonstrated by the parallel courses of the concentration curves for Na and Cl and the antiparallel course of the curve for S along the beam scanning line (see Fig. 19, *f*).

The characteristic size of the chemical phases is smaller than the local analysis area, which depends on the electron beam diameter (~2 μm); therefore, all elements can be determined simultaneously at each point

of the sample. With allowance for the above-presented data on the elemental composition of the reaction products, it can be assumed that the product phases observed are formed by several compounds. The "light" region contains mainly Cl (NaCl, chloro derivatives), while the "dark" region contains mainly S (benzenesulfonamide).

Comparison of regions II and III made it possible to monitor the dynamics of structurization during SHS and to propose a mechanism for the interaction between HQ and CA in the SHS wave. On heating, the reactants form a melt whose melting point is lower than the combustion temperature. The melt undergoes capillary spreading in the porous matrix of high-melting CA. During the reaction, the crystal structures of the reactants are entirely destroyed and the texture of the initial mix is disturbed. The subsequent crystallization of the reaction product affords microregions of two types, larger (~5—10 μm) regions containing predominantly Cl or S and smaller regions with a size of <2 μm.

References

1. E. G. Klimchuk, G. M. Avetisyan, and A. G. Merzhanov, *Dokl. Akad. Nauk SSSR*, 1990, **311**, 1161 [*Dokl. Chem.*, 1990 (Engl. Transl.)].
2. E. G. Klimchuk, G. M. Avetisyan, and A. G. Merzhanov, *Zh. Prikl. Khim.*, 1990, **6**, 1436 [*J. Appl. Chem. USSR*, 1990, **6** (Engl. Transl.)].
3. A. G. Merzhanov, in *Fizicheskaya khimiya. Sovremennye problemy* [*Physical Chemistry. Modern Problems*], Ed. Ya. M. Kolotyrkin, 1983, **3**, 6 (in Russian)
4. I. P. Borovinskaya, *Pure and Appl. Chem.*, 1992, **64**, 919.
5. A. G. Merzhanov, *Internat. J. of Self-Prop. High-Temp. Synt.*, 1993, **2**, 113.
6. A. G. Merzhanov, *Comb. Sci. T.*, 1994, **98**, 307.
7. E. G. Klimchuk and A. G. Merzhanov, *Fizika Goreniya i Vzryva* [*Combusion and Explosion Physics*], 1990, **6**, 104 (in Russian).
8. A. B. Kitaigorodskii, *Molekulyarnye kristally* [*Molecular Crystals*], Nauka, Moscow, 1971 (in Russian).
9. A. R. West, *Solid State Chemistry and Its Applications*, J. Wiley and Sons, Chichester—New York, 1984.
10. C. N. R. Rao and J. Gopalakrishnan, *New Directions in Solid State Chemistry*, Cambridge University Press, Cambridge—London—New York, 1986.
11. E. G. Klimchuk, K. G. Gazaryan, and A. G. Merzhanov, *Fizika Goreniya i Vzryva* [*Combusion and Explosion Physics*], 1991, **5**, 91 (in Russian).
12. A. G. Merzhanov, V. L. Dragun, B. M. Khusid, E. G. Klimchuk, S. A. Filatov, and V. V. Sen'kov, *Inzhenerno-Fizicheskii Zhurn.* [*Eng. Phys. J.*], 1990, **6**, 943 (in Russian).
13. V. I. Ponomarev, E. G. Klimchuk, A. G. Merzhanov, and O. S. Filipenko, *Izv. Akad. Nauk, Ser. Khim.*, 1997, 979 [*Russ. Chem. Bull.*, 1997, **46**, 939 (Engl. Transl.)].
14. E. G. Klimchuk, A. A. Khodak, and A. G. Merzhanov, *Izv. Akad. Nauk, Ser. Khim.*, 1999, 301 [*Russ. Chem. Bull.*, 1999, **48**, 300 (Engl. Transl.)].
15. *Kratkaya khimicheskaya entsiklopediya* [*Concise Chem. Encyclopedia*], Sovetskaya entsiklopediya, Moscow, 1967, **5**, 699 (in Russian).
16. R. G. W. Hollingsched, *Oxine and Its Derivatives*, London, 1954—1956, **1**—**4**.
17. A. V. Vinogradov and S. V. Elinson, *Oksikhinolin* [*Hydroxyquinoline*], Nauka, Moscow, 1979 (in Russian).
18. *Tablitsy fizicheskikh velichin. Spravochnik* [*Tables of Physical Quantities*], Ed. I. K. Kikoin, Atomizdat, Moscow, 1976, p. 185 (in Russian).
19. J. P. Phillips, E. M. Barrall, and R. Brees, *Trans. Kentucky Acad. Sci.*, 1956, **17**, 135; *Chem. Abstrs.*, 1957, **51**, 11349b.
20. *Khromatografiya v tonkikh sloyakh* [*Thin-Layer Chromatography*], Ed. E. Schtal, Mir, Moscow, 1965, p. 48 (Russ. Transl.).
21. W. Jones and J. M. Thomas, *Progr. Solid St. Chem.*, 1979, **12**, 101.
22. V. A. Batyrev, *Rentgeno-spektral'nyi elektrozondovyi mikroanaliz* [*X-Ray Spectral Electron Probe Analysis*], Metallurgiya, Moscow, 1982, 151 pp. (in Russian).
23. J. Boerio-Goates, J. I. Artman, and D. Gold, *J. Phys. Chem. Solids*, 1987, **48**, 1185.
24. *Khimicheskii entsiklopedicheskii slovar'* [*Chemical Encyclopedic Dictionary*], Sovetskaya entsiklopediya, Moscow, 1983, 353 (in Russian).
25. N. P. Novikov, I. P. Borovinskaya, and A. G. Merzhanov, *Fizika Goreniya i Vzryva* [*Combusion and Explosion Physics*], 1974, **10**, 201 (in Russian).
26. A. G. Merzhanov, *Comb. Flame*, 1969, **2**, 143.
27. K. G. Shkadinskii, B. I. Khaikin, and A. G. Merzhanov, *Fizika Goreniya i Vzryva* [*Combusion and Explosion Physics*], 1971, **7**, 19 (in Russian).
28. Ya. B. Zel'dovich, O. I. Leipunskii, and V. B. Librovich, *Teoriya nestatsionarnogo goreniya porokha* [*Theory of Non-Steady-State Powder Combustion*], Nauka, Moscow, 1975 (in Russian).
29. A. P. Aldushin, *Fizika Goreniya i Vzryva* [*Combusion and Explosion Physics*], 1982, **3**, 47 (in Russian).
30. J. Murase and Y. Demura, *Met. Fac. Sci., Kyushu Univ. Ser.*, 1961, **C4**, 175; *Chem. Abstrs.*, 1963, **58**, 3390b.
31. R. L. Shriner, R. C. Fuson, D. Y. Curtin, and T. C. Morrill, *The Systematic Identification of Organic Compounds, Lab. Manual*, J. Wiley and Sons, New York, 1980.
32. S. Katayama, Y. Akahori, and H. Mori, *Chem. Pharm. Bull.*, 1973, **21**, 2622.
33. *Khimicheskaya entsiklopediya* [*Chem. Encyclopedia*], Sovetskaya entsiklopediya, Moscow, 1988, **1**, 133 (in Russian).
34. *UV Atlas of Organic Compounds*, Verlag Chemie, Butterworths, 1966.
35. A. L. Buchachenko and A. Vasserman, *Stabil'nye radikaly* [*Stable Radicals*], Khimiya, Moscow, 1973 (in Russian).
36. S. Auricchio, M. Bianca, A. Gitterio, F. Minisci, and S. Ventura, *Tetrahedron Lett.*, 1984, **25**, 3373.
37. A. R. Katritzky and J. M. Lagowski, *Chemistry of the Heterocyclic N-Oxides*, Academic Press, London—New York, 1971.
38. R. P. Tsivilev, *Izv. Akad. Nauk SSSR. Neorgan. Mater.* [*Bull. USSR Acad. Sci. Inorg. Mater.*], 1986, **22**, 442 (in Russian).
39. D. A. Frank-Kamenetskii, *Diffuziya i massoperenos v khimicheskoi kinetike* [*Diffusion and Mass Transfer in Chemical Kinetics*], Nauka, Moscow, 1982 (in Russian).
40. R. P. Rastogi, N. B. Singh, and R. P. Singh, *Indian J. Chem., A*, 1977, **15A (II)**, 941.
41. R. Schollhorn, *Pure and Appl. Chem.*, 1984, **56**, 1739.
42. V. A. Zlobin, *Kinet. Katal.*, 1985, **26**, 458 [*Kinet. Catal.*, 1985, **26** (Engl. Transl.)].

Received December 27, 1996;
in revised form April 9, 1999